Cerebral Cortex, 2016, 1–15

doi: 10.1093/cercor/bhv331
Original Article

ORIGINAL ARTICLE

Disrupted Cortical State Regulation in a Rat Model of Fragile X Syndrome

Julia Berzhanskaya[1], Marnie A. Phillips[1], Alexis Gorin[2], Chongxi Lai[2], Jing Shen[2] and Matthew T. Colonnese[1]

[1]Department of Pharmacology and Physiology and Institute for Neuroscience and [2]Department of Electrical Engineering, School of Engineering and Applied Sciences, The George Washington University, Washington, DC 20052, USA

Address correspondence to Matthew T. Colonnese, 2300 Eye St NW, Ross Hall 640, Washington, DC 20037, USA. Email: colonnese@gwu.edu

Abstract

Children with Fragile X syndrome (FXS) have deficits of attention and arousal. To begin to identify the neural causes of these deficits, we examined juvenile rats lacking the Fragile X mental retardation protein (FMR-KO) for disruption of cortical activity related to attention and arousal. Specifically, we examined the switching of visual cortex between activated and inactivated states that normally occurs during movement and quiet rest, respectively. In both wild-type and FMR-KO rats, during the third and fourth postnatal weeks cortical activity during periods of movement was dominated by an activated state with prominent 18–52 Hz activity. However, during quiet rest, when activity in wild-type rats became dominated by the inactivated state (3–9 Hz activity), FMR-KO rat cortex abnormally remained activated, resulting in increased high-frequency and reduced low-frequency power during rest. Firing rate correlations revealed reduced synchronization in FMR-KO rats, particularly between fast-spiking interneurons, that developmentally precede cortical state defects. Together our data suggest that disrupted inhibitory connectivity impairs the ability of visual cortex to regulate exit from the activated state in a behaviorally appropriate manner, potentially contributing to disrupted attention and sensory processing observed in children with FXS by making it more difficult to decrease cortical drive by unattended stimuli.

Key words: attention, autism, cortex, development, EEG

Introduction

Loss of function mutations in *FMR1* leading to loss of the FMR protein (FMRP) are the primary cause of the cognitive, physical, and behavioral impairments characteristic of Fragile X syndrome (FXS) (Jacquemont et al. 2007). As a translation repressor, FMRP regulates over 800 gene products in the developing mouse brain (Darnell and Klann 2013). Determining the paths leading from this primary disruption of translation to the onset of neurological symptoms is critical for treatment development. Because FMRP is expressed embryonically, the complexity of this relationship is likely to increase over time as secondary alterations in translation and circuits occur. Developmental approaches are thus important to understand the initiation and progression of disease, its convergence with other neurodevelopmental disorders such as autism spectrum disorders (ASD), and eventually target therapeutic interventions to the age at which they are likely to be most effective, even if presymptomatic (Meredith et al. 2012). Key to this task is identifying the alterations in behaviorally relevant neural activity in developing animal models of FXS that are comparable with the human disease (Wijetunge et al. 2013).

Abnormal attention is a core deficit in children with FXS, and an inability to modulate arousal has been proposed as a key mechanistic defect underlying the attention phenotype of FXS patients (Cornish et al. 2004). A few key studies show arousal and attention deficits in Fmr1 mutant mice (Moon et al. 2006, 2008; Krueger et al. 2011; Kramvis et al. 2013). However, tests that more directly assay the cortical processing involved in

attention and arousal and that have obvious homology to humans are needed to understand how reduced FMRP levels influence behavior. Examining the spontaneous modulations of the electroencephalogram (EEG) in the absence of a specific task (rest) is a promising possibility, as FXS children show an increase in activity frequencies related to attention and arousal when at rest (Van der Molen and Van der Molen 2013).

A wealth of recent studies have revealed modulations of spontaneous activity in wild-type mouse sensory cortex related to their level of arousal and active sensing (McCormick et al. 2014). These are similar to modulations observed in primates as they shift attention between spatial locales (Fries et al. 2001), and thus are likely cellular and network models of this process (Harris and Thiele 2011). During arousal and active sensing, for example when whisking (somatosensory cortex) (Poulet and Petersen 2008) or moving (visual cortex) (Niell and Stryker 2010; Polack et al. 2013), the relevant primary sensory cortex enters an "activated" (also called desynchronized) state in which balanced excitatory and inhibitory activity stably depolarizes neurons (Poulet and Petersen 2008; Haider and McCormick 2009; Polack et al. 2013). As a result, low-frequency power is reduced in the local EEG signal. In visual cortex, the activated state increases signal to noise (Niell and Stryker 2010; Reimer et al. 2014; Vinck et al. 2015), presumed to be beneficial for attending to appropriate stimuli. As active sensing and arousal wane, the cortex enters an inactivated (synchronized) state in which synchronized hyperpolarizations of membrane potential lead to large, slow fluctuations in the population firing rate and EEG signal. Cortical networks are hyperexcitable in the absence of FMRP (Contractor et al. 2015), but observed changes in spontaneous activity have so far been limited to synchronized states (Hays et al. 2011; Goncalves et al. 2013), making it unclear how circuit hyperexcitability in FXS contributes to attention deficits in FXS.

Here, we address this question in the visual cortex of developing infant and juvenile Fmr1 mutant rats (FMR-KO) allowed to cycle freely between quiet waking and moving. We chose to examine the early visual cortex for multiple reasons. Defects in visual attention are among the earliest to appear in FXS (Scerif et al. 2004; Roberts et al. 2012) as well as ASD (Zwaigenbaum et al. 2005). Examination of visual cortex allows internal changes resulting from state modulation to be separated from changes due to sensory input, which is difficult in somatosensory cortex. Using multielectrode array recordings of depth EEG (dEEG), as well as single-unit activity and multiunit activity (MUA), allows characterization of cortical activity translatable to human EEG, while examining the neuronal basis of these behaviors. Furthermore, the size and robustness of the young rat and the fact that it is born at an earlier developmental stage than the human, offers an advantage in developmental studies. Our extensive earlier work has characterized in detail the development of activity in rat visual cortex in vivo, and identified similar changes in the EEG of human infants born preterm (Colonnese and Khazipov 2012). This work identified eye-opening in rats as the equivalent stage to human birth for visual cortex. It was not until the recent creation of FMR-KO rats that this detailed normal timeline could be applied to models of neuro-developmental disorders.

FMR-KO rats recapitulate spine density and synaptic plasticity defects observed in some mouse models, are deficient in hippocampal forms of associative recognition memory (Till et al. 2015), and display novel social interaction phenotypes (Hamilton et al. 2014). Here, we show a normal timeline for development of several important milestones in cortical maturation, including development of continuous spontaneous activity (Colonnese et al. 2010). We do identify critically deficient regulation of cortical states that appears during the developmental period prior to the observation of FXS symptoms in humans and may link hyperexcitability of cortical circuits to behavior deficits of attention and arousal.

Materials and Methods

Animals

All experiments were conducted with approval from The George Washington University School of Medicine and Health Sciences Institutional Animal Care and Use Committee, and in accordance with the *Guide for the Care and Use of Laboratory Animals* (8th Edition, National Academies Press). Sprague-Dawley FMR-KO rats were acquired from SAGE Labs (St Louis MO). Experiments were conducted in 2 separate series. In the 1st series $FMR^{-/-}$ and $FMR^{y/-}$ pups were either shipped at P4 directly from Sage Labs or bred in the local animal facility. Sprague-Dawley rats acquired from Hilltop Lab Animals (Scottdale, PA, USA) in a similar manner were used as wild-type. Both female and male animals were used. A broad range of ages was used in this series as part of a discovery phase to determine age ranges of phenotype effects. In the second series, male mutant and wild-type littermates were obtained by crossing $FMR^{+/-}$ females with wild-type males from Hilltop Labs. Animals were identified and sexed by genotyping for the presence of the mutant or wild-type gene and presence of the Y chromosome (Transnetyx, Cordova, TN, USA). For the second series, the experiments and analysis were performed blind to genotype on both a wild-type and an FMR-KO littermate on the same or subsequent day. Ages of these animals were restricted to particular ages of interest, P5–6, P9–11, and P19–24 based on the first series. The mean age for second-series juveniles was 22.4 ± 2.1 standard deviation (SD) for WT and 21.6 ± 2.0 SD for FMR-KO. Analyses of juvenile animals are reported exclusively for the second series of animals, except for the developmental analysis (Fig. 2E) which combines groups. For infants (<P12), the 2 groups were analyzed separately, determined to have means that were not significantly different, and combined for the final analysis. For movement analysis (Fig. 1), only animals with no movement artifacts in the dEEG were used.

Surgery and Recordings

Recording methodology has been described previously (Colonnese et al. 2010; Colonnese 2014). For installation of the head-fixation apparatus, animals were given subcutaneous carprofen injections (5 mg/kg weight) and anesthetized at 2–3% isoflurane. Adequate depth of anesthesia was verified by toe pinch and breathing rate. Resection of the scalp was made using aseptic technique, the skull was cleaned of connective tissue, and electrode locations were marked on the skull. A head-fixation bar and vertical frontal mounting pole were attached to the skull with dental cement, leaving the recording window free of cement.

For recording, under isoflurane anesthesia, the animal was placed in a modified stereotaxic apparatus that attached to the headgear. Body restraint was provided by soft sterile cloth-lined tube. Body temperature (measured under the abdomen) was maintained between 32 and 36°C via an electric heating pad placed under the tube. Monocular visual cortex was targeted with the following coordinates: 0–0.5 mm anterior from *lambda* and 2.5 (P4–5), 2.8 (P9–11), or 3.0–3.5 (P13+) lateral. An Ag/AgCl wire was placed over right frontal cortex (~1 mm anterior and 3 mm lateral to bregma) as ground. The skull over frontal pole (for ground insertion) and over visual cortex was thinned until

transparent. The final layer of bone was chipped until producing a craniotomy 100–200 μm diameter. In older animals the dura was resected. A stainless steel wire (100 μm diameter) was placed in the facial muscle for electromyography (EMG), and a piezoelectric motion detector was placed under the animal to monitor body motion.

Neural activity was recorded using Neuronexus (Ann Arbor, MI, USA) 32-channel probes, positioned radially to the cortical layers using a micromanipulator. Either a "Poly2" design of 2 parallel rows of 16 sites, separated by 50 μm, which allowed for simultaneous recording of layers 2–5 for dEEG as well as tetrode-based spike-sorting, or a linear array with 50-μm separation, which allowed for more precise identification of the input layer was used. Spectral analysis of resting-state activity P16–30 combined recordings from Poly2 and linear arrays, as the mean spectral distributions for these probes did not differ. All electrodes were coated in DiI (Sigma, St Louis, MO, USA) to allow postexperiment penetration localization.

Electrical signals were collected using Neuralynx (Bozeman, MT, USA) Digital Lynx S hardware with Cheetah (v5.5) software. dEEG signals were band-pass filtered between 0.1 Hz to 9 kHz, and digitized at 32 kHz. All recordings were referenced to the bottom electrode to eliminate large slow potential variations and common mode noise. Spikes were extracted by threshold crossing of −40 μV in the 600 Hz–9 kHz band-pass signal, and saved as 1-ms, 32-point waveforms for all 4 electrodes in the designated tetrode.

Data Analysis

Neural signals were imported into Matlab (Mathworks, MA, USA). dEEG was down-sampled to 1 kHz. Layer 4 was identified in each recording as the layer with the earliest negative deflection in the mean visual evoked response. Location relative to the electrode with the highest firing rate (Layer 5a) as well as absolute depth from the cortical surface (at least 350 μm) were used to resolve ambiguity. Periods of sleep, defined as the absence of movement or EMG signal for longer than 5 min, were removed, and the remaining portion was divided into 3 behavioral epochs: moving, whisking/chewing, quiet wakefulness. "Moving" periods consisted of piezo signal above threshold indicating volitional movement of the trunk and limbs. "Whisking/chewing" consisted of low piezo signal but EMG above threshold indicating activation of the facial muscles without large body movements. Observation of the animals showed this included whisking, repetitive chewing, and grooming. "Quiet wakefulness" consisted of piezo and EMG both below threshold. Spot check of the animals indicated eyes were open throughout these periods. Threshold for each channel were defined by the Teager–Kaiser energy operator (Solnik et al. 2010) exceeding by 3 SDs from the mean signal. Periods of quiet wakefulness <2 s duration were reclassified as moving or whisking/chewing based on the surrounding behaviors. Animals were eliminated if more than 50% of time segments were contaminated by motion artifact.

Approximately 25% of animals expressed 2–4 Hz high-voltage spike-wave complexes (Steriade et al. 1994) that are commonly detected in Sprague-Dawley rats (Pearce et al. 2014). In the first group of experiments, this activity was linked to genotype, with 12% of wild-type but 43% of FMR-KO rats displaying spike-wave discharges for longer than 10 s. In the second group of experiments, sharp wave activity was not linked to genotype, and occurred in 24% and 28% of FMR-KO and wild-type animals, respectively. Periods including spike-wave discharges were excluded from analysis by elimination of all 1-min periods containing dEEG activity >600 μV.

dEEG Spectral Analysis

For spontaneous activity, dEEG traces were segmented into fixed length records (1 s long for P13–30, 3 s for P4–11). dEEG spectra were obtained by multitaper method using the freely available Chronux package (Mitra and Bokil 2007) with taper parameters [3 5]. Multitaper spectra were multiplied by frequency^2; frequency resolution was resampled on a log scale to equalize the representation of high and low frequencies in the spectra and reduce the multiple comparisons problem; finally, frequency power was normalized in each window by z-score transform of the spectra between 1 and 100 Hz.

Single- and Multiunit Analysis

Putative single-unit isolation was done based on spike shapes using the masked EM algorithm (Klustakwik; (Kadir et al. 2014)) in Peak, Energy, PCA2 space for all 4 electrodes in each tetrode. Clusters were further refined based on shape similarity of spikes in a cluster using custom written Matlab code. For each spike in a cluster, the mean Euclidian distance from the mean spike waveform $|x - \bar{x}|$ was calculated, where x is the individual spike waveform, $\bar{x}$ is average spike waveform for the cluster. The similarity metric is then computed as follows:

$$\mathrm{Sim} = \left(1 - \frac{|||\mathbf{x} - \bar{\mathbf{x}}|||}{\max(||\mathbf{x}||, ||\bar{\mathbf{x}}||)}\right). \quad (1)$$

Spikes that had a similarity of less than 0.58 were removed from the cluster. The mean "Similarity" of all spikes in a cleaned cluster was then used to evaluate clusters for inclusion of only a single unit. Visual inspection of >100 clusters determined a mean Similarity of >0.58 to correspond to a human observer's opinion of a waveform distribution generated by a single neuron. Clusters were included in the analysis with the following minimal measures (Schmitzer-Torbert et al. 2005): "Isolation distance" > 15, $L_{\mathrm{ratio}} < 0.5$, percentage of spikes with an interspike interval below 2 ms <1%, mean similarity > 0.58, and number of spikes >60. With this method, 60–80% of all spikes were assigned to good clusters and included in the analysis. Further visual inspection of spike clusters was used to eliminate clusters with average waveforms that were distorted or contained electrical artifacts (<1% of all isolated units). To split clusters into functional neuron classes, we measured peak-valley ratio, peak-valley delay, and relative repolarization within 500 ms of peak. Three-dimensional hierarchical clustering identified 2 groups, which could be separated by repolarization threshold alone (Fig. 3A,B). Neurons with low repolarization (<0.58) were classified as regular-spiking (RS) cells, those above this threshold as fast-spiking (FS).

Single-unit pair-wise spike correlations were calculated with the method of Renart et al. (2010) with $T = 25$ ms and $J = 250$ ms. This measures correlation in spike rates smoothed by a Gaussian kernel with SD 25 ms, with the effect of slow correlations (>J) removed. Jittered spike correlations were made from random spike trains with the same spike rate as the original unit. The proportion of anticorrelated and positively correlated pairs was calculated as the proportion of pairs with correlation coefficients below or above 0.04 (3 SDs from jittered mean) after subtraction of the proportion of jittered pairs below or above the same threshold. Periods of activation were defined from the normalized LFP

power in 1 s windows containing normalized 4–8 Hz power <0 and 25–50 Hz power >0 (Fig. 2C,D).

Multiunit correlations were computed using the standard formula with normalization leading to autocorrelation $CCF(y,y)_{dt=0}=1$;

$$CCF_{raw}(y1,y2)_{dt}=\frac{1}{\sqrt{a1\times a2}}\sum_{t=0}^{T-dt} y1_t y2_{t+dt}, \quad (2)$$

where $a1$ and $a2$ are normalization coefficients that bring autocorrelations of spike trains $y1$ and $y2$ to 1 at $dt=0$. To correct for firing rate and remove the effects of slow correlation, 20 jittered spike trains were generated with the spikes moved by a random factor between −250 and 250 ms and the average CCF of these jittered trains was subtracted from the raw correlation:

$$CCF_{corr} = CCF_{raw} - <CCF_{rand}> \quad (3)$$

Event duration was calculated by summing multiunit spike occurrence across all channels and defining events as containing at least 2 spikes separated by <500 ms.

Statistics

Distributions were evaluated for normality using the Anderson–Darling test. Normally distributed data are reported as mean ± standard error of the mean. Non-normal data are reported as median ± standard error of the median as determined by bootstrapping (1000 iterations). Spectra were examined at each frequency for significant difference using nonparametric permutation tests corrected for multiple comparisons by the method of Cohen (2014). All other tests are described in the Results and performed in Matlab.

Results

In order to approximate studies of resting-state activity in humans, cortical activity was monitored with multielectrode arrays to record dEEG signal-unit activity and MUA from all layers of monocular primary visual cortex (V1) in head-fixed, unanesthetized rats maintained in low-light conditions, with no specific visual stimulation. Under these conditions, wild-type rats P14–30 ($n=39$) spent 11 ± 10% (SD) of their time making volitional movements of the limbs and trunk, 17 ± 11% of their time whisking and chewing without trunk movement, and the remainder in "quiet wakefulness" (absence of volitional body movements). The behavior of FMR-KO rats ($n=45$) was similar: 12 ± 10% time moving and 16 ± 15% whisking/chewing (data not shown).

Normal Movement-Related Modulation of Cortical Activity in Head-Fixed Developing Rats

We first determined whether body movements in male wild-type juvenile rats during ages roughly equivalent to human infancy (P19–24) were associated with changes in cortical state similar to those observed in wild-type mice (Niell and Stryker 2010) (Fig. 1A). At this age, the development of cortical active states has stabilized (Colonnese 2014) and FS and RS neurons can be separated, but movement-dependent gamma oscillations, indicative of adult cortical activity, have not emerged (Hoy and Niell 2015). For this analysis, we used littermate paired males, and excluded pairs with any movement-induced artifacts in the dEEG ($n=14$). In the head-fixed, wild-type rats, periods with no overt body movements (quiet wakefulness) were associated with a dEEG dominated by large amplitude low-frequency activity, a pattern of activity called the "inactivated" or "desynchronized" state (Harris and Thiele 2011; McCormick et al. 2014). During and immediately surrounding movement periods, low-frequency power was attenuated and high-frequency power increased, a pattern called the "activated" or "synchronized" state. The population means of normalized spectra from 1-s windows that included movement were significantly different from those that did not in 2 broad frequency bands (Fig. 1C1). Pair-wise comparison at all frequencies (permutation analysis $P<0.01$ with multiple comparisons correction) revealed that all frequencies from 3.7 to 8.6 Hz were significantly reduced by movement, while all frequencies from 24.4 to 51.8 Hz were significantly increased. To determine whether this modulation occurred similarly in individual animals, we determined the frequencies significantly modulated by movement in each animal (Fig. 1C2). Of the 14 wild-type animals examined, all had multiple frequencies below 10 Hz negatively modulated by movement and multiple frequencies above 20 Hz that were positively modulated. Thirteen of the 14 wild-type animals modulated cortical activity in larger frequency bands than revealed by the population average, suggesting that simple mean normalization does not adequately control variability among animals. To further control variability, visualize frequency differences without the dominant and constant $1/f$ frequency relationship, and better compare spectra in single time windows across animals, we removed the $1/f$ power relationship and then normalized the spectral distribution using a z-score transform. Population spectral average for this normalized frequency distribution was significantly modulated by movement more similarly to that of the individual animals (Fig. 1C3). All frequencies between 2.8 and 9.5 Hz were reduced by movement, while all frequencies between 18.4 and 51.8 Hz were increased (permutation analysis $P<0.01$). Thus, head-fixed wild-type rats modulate cortical activity in a manner similar to wild-type mice on treadmill (Hoy and Niell 2015).

Disrupted Modulation of Cortical States in Juvenile FMR-KO Rats

Age-matched male FMR-KO littermates ($n=14$) showed no significant modulation of the dEEG between movement and quiet wakefulness (Fig. 1B). During both behavior states, the dEEG was dominated by low-amplitude high-frequency activity. The population mean spectra for relative power (Fig. 1D1) and z-score normalized power (Fig. 1D3) contained no frequencies that were different between movement and quiet rest. Only one FMR-KO rat showed the wild-type pattern of reduced low frequencies and increased high frequencies during movement (Fig. 1D2). However, 9 showed at least one high-frequency band significantly increased during movement, suggesting modulation of these frequencies by movement is less affected than the low frequencies in FMR-KO rats.

In mice, cortical activation can occur during periods of arousal even in the absence of movement (Vinck et al. 2015). Activation in the absence of movement reduces spike rates, while movement increases them. In contrast to our dEEG results, normal modulation of spiking activity by movement was unaffected in FMR-KO rats (Fig. 1E). MUA in wild-type animals was 21 ± 5% greater during movement than during quiet wakefulness ($P=0.0014$, one-sample t-test for difference from zero). In FMR-KO rats MUA increased by a comparable amount, 18 ± 6% ($P=0.0016$ for difference from zero; $P=0.62$, t-test for difference from wild-type), but their activation score was unchanged after movement ceased. Thus, FMR-KO rats appear to remain in the activated "aroused"

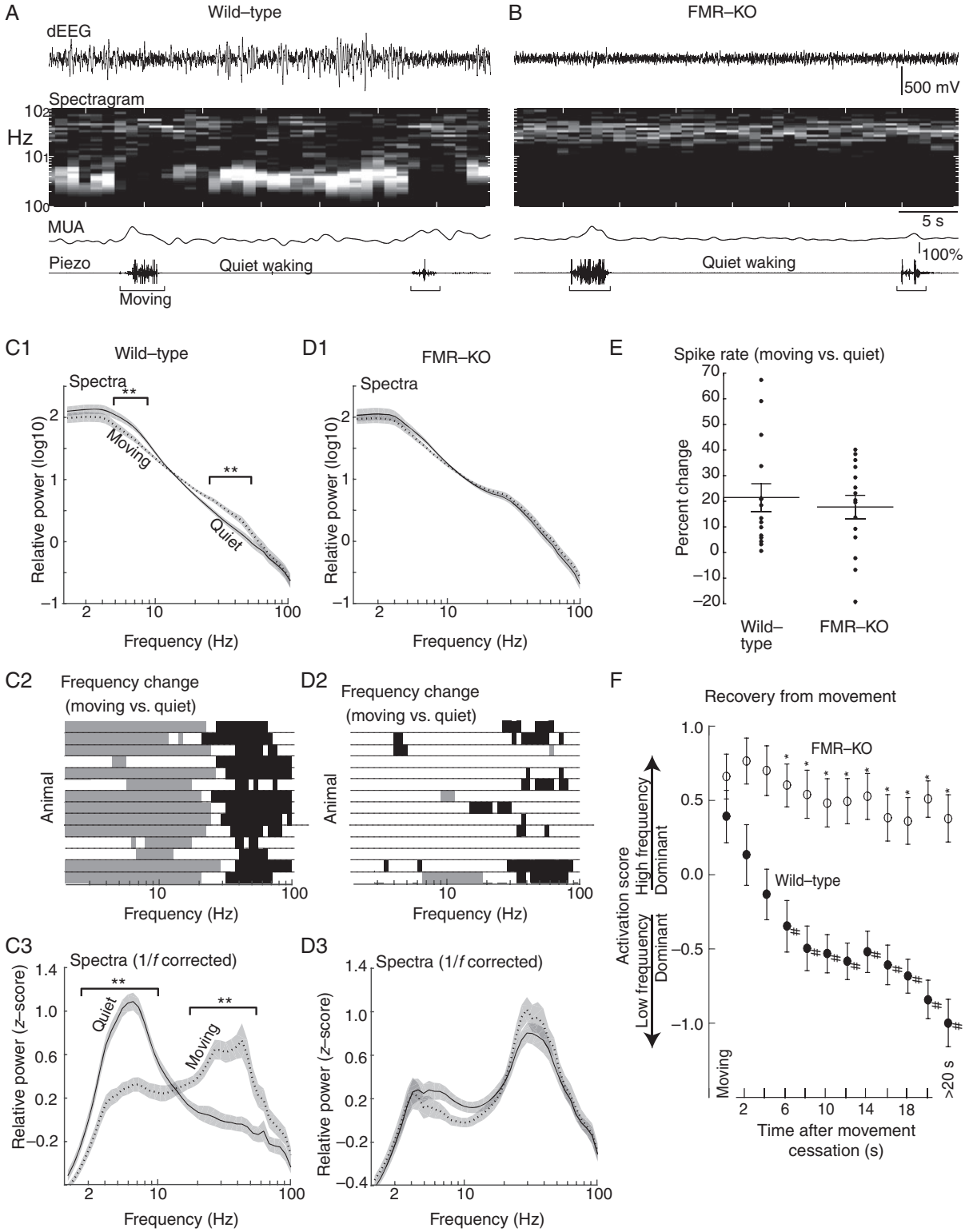

Figure 1. Impaired movement-related cortical state regulation in FMR-KO rats. (*A*) Example depth electroencephalogram (dEEG) and associated time-spectrogram from superficial layers of a P22 wild-type rat. Below are associated multiunit activity (MUA) from all layers and piezo-derived movement signal. Note reduced 2–8 Hz signal and increased MUA during movement. (*B*) Example from a P22 FMR-KO. (*C*) P19–24 modulation by behavioral state of male wild-type rats ($n = 14$). (*C1*) Population mean spectra during movement and during quiet (waking) periods. Square brackets show frequencies with significant difference between conditions ($P < 0.01$ permutation analysis). (*C2*) Individual animal responses in rows. Gray bars show frequencies with significant negative modulation by movement; black bars significant positive modulation. (*C3*) Population mean spectra in which the 1/f relationship has been removed and the spectra z-score normalized. Square brackets show frequencies with significant difference. (*D*) P19–24 modulation by behavioral state for male littermate FMR-KO rats ($n = 14$). (*E*) Modulation of MUA by movement. (*F*) Time course of the shift between activated and inactivated states after cessation of movement. "Activation Score" is measured as mean 25–50 Hz relative power – mean 4–8 Hz relative power. >20 s means all times more than 20 s after movement. *Significant differences between groups, #significant difference from Moving timepoint in same group ($P < 0.01$ by pair-wise analysis following mANOVA).

state during quiet wakefulness, rather than the movement-dependent state.

In mice, low-frequency activity increases and high-frequency activity decreases within seconds after the cessation of movement. This is followed by a second, slower, shift over the next 10–30 s (Vinck et al. 2015). To determine whether an extension of the recovery time in FMR-KO rats is responsible for the observed lack of cortical state modulation by movement, we examined the shift in dEEG frequencies as a function of time after movement cessation (Fig. 1F). To compare frequency distributions, an "Activation Score" was calculated which represents the distance between mean relative power in the high and low frequency maximally modulated by movement (4–8 and 25–50 Hz, respectively). During movement Activation Scores were not significantly different between wild-type and FMR-KO (WT 0.33 ± 0.18; FMR-KO 0.54 ± 0.15; $P = 0.31$ t-test). After cessation of movement, wild-type Activation Scores were rapidly reduced (less-activation), while FMR-KO scores remained constant. mANOVA analysis reveals effects of group ($P < 10^{-30}$) and time ($P = 0.0018$), as well as an interaction between the two ($P = 0.04$). Pairwise post hoc analysis (Tukey HSD, $P < 0.05$) showed that Activation Scores in wild-type animals became significantly different from movement after 6–7 s, and remained unchanged after this. In contrast, FMR-KO showed no significant modulation of Activation Score. Wild-type and FMR-KO Activation Scores were significantly different from each other all times between 4 and 20 s after movement, as well as for all nonmovement periods (WT −1.00 ± 0.16; FMR-KO 0.38 ± 0.16; $P = 1.77 \times 10^{-7}$). Thus, the lack of modulation by movement in FMR-KO is not a result of a slowed return to the inactivated state following movement, but rather a persistent increase in the presence of cortical activation during quiescent wakeful periods.

Persistent Activation of Visual Cortex in FMR-KO Rats at Rest

To test the hypothesis that the lack of cortical state modulation in FMR-KO rats results from an increased propensity to remain in the activated state during periods of rest and visual disengagement, we examined cortical activity during periods without movement. This allowed us to include animals with movement-related artifacts increasing the number of age-matched male animals analyzed ($n = 22$ WT and $n = 21$ FMR-KO P19–24). To control for potential differences between groups in the level of systemic arousal during quiet wakefulness, we divided the periods without overt trunk movements into quiet waking (no activity of facial muscles) and whisking/chewing (EMG activity in facial muscles), indicative of arousal without engagement of vision. Under the conditions of our experiment, wild-type rats have an inactivated visual cortex with spectral characteristics similar to quiet wakefulness while engaging in these facial movements (Fig. 2A,B). In contrast, FMR-KO rats in both conditions showed reduced power at all frequencies between 3.3 and 11.5 Hz, and elevated power at all frequencies between 18.4 and 68.7 Hz ($P < 0.01$ permutation test). Thus with similar levels of behavioral arousal, cortical activation patterns were different between the groups.

The changes in frequency power we observe in FMR-KO animals at rest could result from changes in the amplitude of dEEG oscillations, or from a greater proportion of time spent in an activated state that is otherwise normal. To distinguish between these possibilities, we examined the relationship between frequency bands with the greatest difference between moving and quiet wakefulness for each 1 s window used in the analysis of

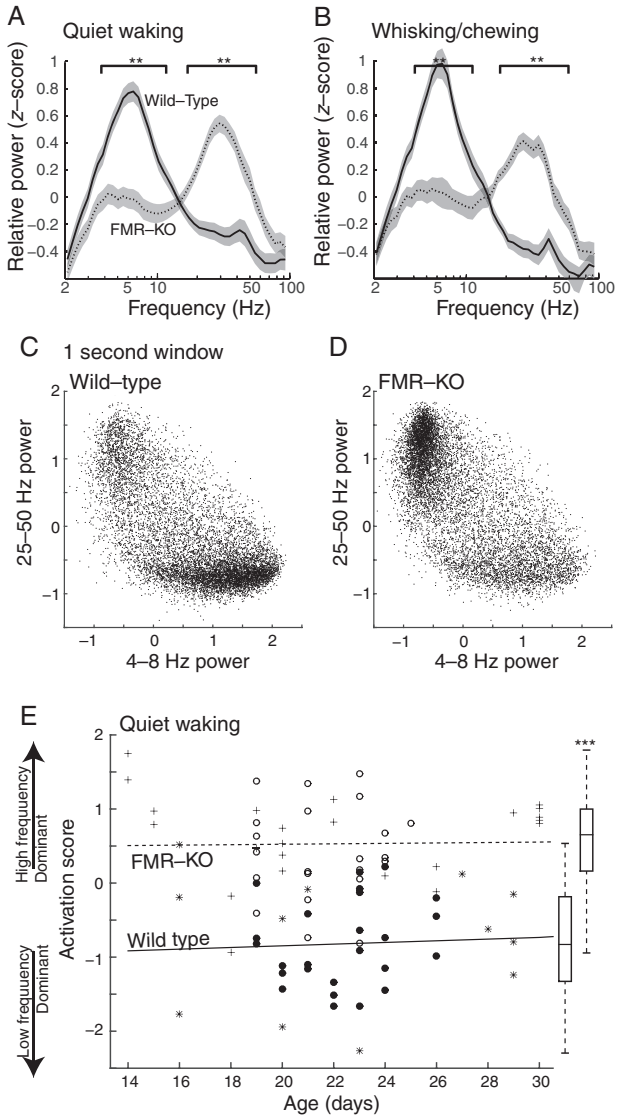

Figure 2. Visual cortex of FMR-KO rats remains in the activated state during visual rest. (*A*) Spectral analysis of juvenile rats (P19–24) during periods of quiet wakefulness. Plots show population mean and standard error of the frequency distribution of the dEEG. Square brackets designate frequencies with significant differences between groups ($P < 0.01$ permutation analysis). Data are from male wild-type ($n = 22$) and FMR-KO littermates ($n = 21$). (*B*) Spectral analysis of animals during whisking or chewing, a sign of behavioral arousal without visual engagement. (*C*,*D*) Frequency relationships for all 1-s windows used in A. Mean normalized low-frequency (4–8 Hz) power on the *x*-axis versus high-frequency (25–50 Hz) power on the *y*-axis. The plot shows that the increased high-frequency power seen in FMR-KO rats results from more time spent in the activated state, rather than a generalized increase in power at high frequencies. (*E*) Activation Score for all animals P14–30 during quiet waking. Filled circles and asterisks are wild-type; empty circles and plus signs are FMR-KO. Circles are male littermates (Experiment 2); asterisks and plus signs are male and female animals from different litters (Experiment 1). Lines show linear regressions for each group. Box plot shows median, 75 percentile (box), and range (line) for P14–30 ($P < 10^{-14}$).

quiet waking. The distribution of powers in each window revealed 2 clear states that were similar for each genotype, but differed in the amount of time the genotype spent in each (Fig. 2C,D). Wild-type rats spent the majority of their time during quiet wakefulness with high 4–8 Hz and low 25–50 power (inactivated state). FMR-KO rats, in contrast, spent most of their time with high 25–50 Hz and low 4–8 Hz power (activated state). 25–50 Hz

power in windows with low 4–8 Hz power was not significantly elevated for FMR-KO animals compared with wild-type, indicating that the 2 groups are both capable of producing similar cortical states, but differ in the amount of time spent in each.

The development of cortical active states is delayed in organotypic cultures of FMR mutant mice (Motanis and Buonomano 2015). To determine whether a similar delay occurs in vivo, and whether cortical activity defects in FMR-KO are apparent from the earliest ages at which cortical active states appear at P13–14 (Colonnese 2014), we examined Activation Score during quiet wakefulness beginning at eye-opening (P14) through P30, near the end of the critical period (Fagiolini et al. 1994) (Fig. 2E). This developmental analysis included wild-type and mutant littermate males described above, as well as a second group of pups that included homozygous males and females compared with wild-type rats from different mothers (see Materials and Methods). Differences in Activation score were apparent at P14 and remained constant thereafter. The mean Activation Score during this period for all wild-type animals P14–30 ($n = 39$) was -0.82 ± 0.11. For FMR-KO ($n = 45$) animals mean Activation Score was 0.53 ± 0.09 ($P < 10^{-14}$ t-test). There was no effect of sex on mean Activation score (male WT -0.67 ± 0.28 $n = 7$, female WT -0.81 ± 0.33 $n = 10$, male FMR-KO 0.63 ± 0.19 $n = 24$, female FMR-KO 0.78 ± 0.30 $n = 20$).

In summary, our dEEG recordings show that FMR-KO rats have differences in spontaneous resting-state activity from the earliest timepoint at which cortical activation states are expressed. This abnormal cortical resting-state activity is a result of the failure of FMR-KO rats to maintain a deactivated state when at rest or whisking/chewing (when visual attention is reduced) in a head-fixed apparatus. It is this "failure to inactivate" that results in excessive beta–gamma power and reduced theta power in the resting-state dEEG.

Neuronal Hyposynchrony and Disrupted Inhibitory Neuron Interactions in Juvenile FMR-KO Rats

To determine whether the persistent activation observed in FMR-KO rats is a result of increased beta–gamma synchronization and increased firing (similar to the moving state) or of decreased firing and reduced synchronization (similar to the aroused nonmoving state), we examined the behavior of putative single neurons extracted by spike-sorting from tetrode recordings in layers 2 through 5 in the male littermate pair population between P19–24. To determine the contribution of changes in excitatory and inhibitory neuron behavior to the dEEG, units were divided into 2 groups based on the Peak-Trough delay and repolarization time (Fig. 3A,B): RS, putative excitatory, neurons ($n = 439$ wild-type units/22 animals, 324

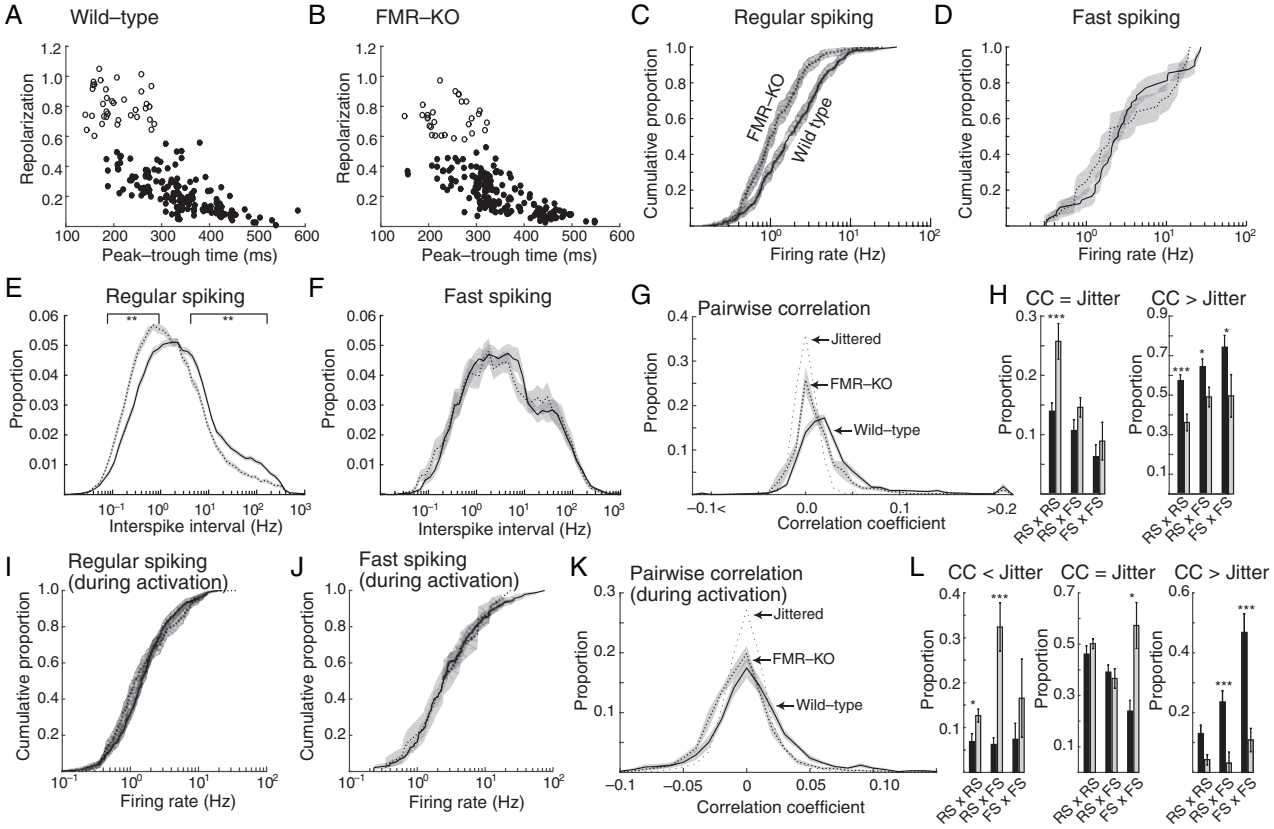

Figure 3. Hyposynchrony and disrupted inhibitory neuron interactions in juvenile FMR-KO rats. Tetrode-based isolation of presumptive single units was used to quantify neuron behavior in juvenile wild-type and FMR-KO (P19-P24). (*A*,*B*) Plot of spike waveforms for 200 neurons of each genotype. Neurons were divided into 2 types based on peak-trough time and repolarization: presumed excitatory regular-spiking (filled circles), and presumed inhibitory Fast-spiking (open circles). (*C*) Cumulative distribution of neuron spike rates of regular-spiking neurons during all cortical states. Shaded regions show 95% confidence interval. (*D*) Firing rates of fast-spiking neurons. (*E*) Population mean of the instantaneous firing rate (interspike interval) distribution of regular-spiking neurons. Line segments show frequency points with significant difference ($P < 0.01$ permutation test) between groups. (*F*) Population mean of instantaneous firing rate distribution for fast-spiking neurons. (*G*) Population mean of the distribution of pair-wise spike rate correlation coefficients during all cortical states. The correlation of jittered units (showing the expected distributions from random firing) is shown as a thin dotted line. (*H*) Population mean of the proportion of units that were not correlated (correlation coefficient [CC] within range of jittered spike distribution) (left) and for units that were correlated (CC higher than the range of the jittered spike distribution) (right). (*I*) Cumulative distribution of neuron firing rates for regular-spiking neurons during the activated state. (*J*) As in (*I*) for fast-spiking neurons. (*K*) As in (*G*) but limited to activated states. (*L*) As in (*H*) but limited to activated states. Leftmost chart shows proportion of neuron pairs that were anticorrelated (CC below range of jittered spike distribution). $^{***}P < 0.001$, $^{**}P < 0.01$, $^{*}P < 0.05$.

FMR-KO/21 animals) and fast-spiking, putative inhibitory, interneurons ($n = 82$ wild-type, 46 FMR-KO).

The distribution of spike rates, calculated as the median of the intraspike interval, of RS neurons shows a shift toward lower firing rates in FMR-KO animals relative to wild-type (Fig. 3C; $P = 3 \times 10^{-7}$ K-S test). The population median was 1.69 ± 0.16 Hz for wild-type and 1.03 ± 0.09 Hz for FMR-KO ($P = 5 \times 10^{-7}$ Wilcoxon rank-sum test). The distribution of firing rate for fast-spiking neurons was not different between groups (Fig. 3D), nor were the population medians (wild-type 2.55 ± 0.36, FMR-KO 1.97 ± 0.73). To determine whether there were changes in patterns of firing, we examined the distributions of interspike intervals (instantaneous firing rates) for both neuron types. Interspike intervals in FMR-KO rats had a general shift to longer intervals (lower frequency) that was specific to RS neurons (Fig. 3E,F). Thus, the decreased firing rate of FMR-KO rats appears to result from a slowing at all frequency bands, rather than a loss of specific high frequencies.

The increased high frequencies we observe could indicate a hypersynchronous network, with increased beta–gamma synchronization (Herculano-Houzel et al. 1999), or, conversely, hyposynchrony resulting from greater prevalence of the activated state (Renart et al. 2010). To differentiate between these possibilities, we examined the role of FMRP in the development of neuronal synchronization by determining the pairwise correlations of all well-isolated neurons in each animal. Correlation was estimated for a 25-ms window, and the effects of shared modulation of firing rates on the order of 250 ms were eliminated (Renart et al. 2010). The distribution of correlation coefficients for all neurons was shifted toward fewer neuron pairs with positive correlation coefficients in FMR-KO rats (Fig. 3G). We evaluated the effects by cell type by calculating the proportion of neuron pairs with correlation coefficients smaller than chance, and those higher than chance. RS neurons had significantly more uncorrelated pairs (14.0 ± 1.4% wild-type vs. 25.7 ± 3.0% FMR-KO, $P = 5 \times 10^{-4}$ Bonferroni corrected t-test) but the proportion of RS × fast spiking (FS) (10.7 ± 1.8% WT vs. 14.6 ± 1.6 FMR) and FS × FS (6.2 ± 2.1% WT vs. 8.9 ± 1.6 FMR-KO) with low correlation was not altered. The proportion of pairs with high correlation was reduced in FMR-KO rats for all 3 pairs: RS × RS (57.2 ± 3.1% WT vs. 36.2 ± 4.2% FMR-KO, $P = 8 \times 10^{-5}$), RS × FS (64.4 ± 3.9% WT vs. 74.3 ± 5.9% FMR-KO, $P = 0.03$), and FS × FS (74.3 ± 5.9% WT vs. 49.6 ± 10.8% FMR-KO, $P = 0.03$). Thus, the strongest effects in the FMR-KO rats are on RS, primarily excitatory neurons, which have reduced firing rates and are desynchronized at rest in the mutants.

The reduced mean firing rates and pairwise cross-correlation we observed in FMR-KO rats could originate in either changes in the local networks, or be a result of the increased time spent in the activated state. To eliminate the effect of increased activation and reveal changes in single-unit activity during the same cortical states, we recalculated firing rates and synchrony during the activated state in both groups. During the activated state, firing rate distributions of RS (Fig. 3J) and FS neurons (Fig. 3K) were not different between groups, and neither were the population medians (RS: 1.21 ± 0.10 Hz WT vs. 0.98 ± 0.14 FMR-KO; FS: 2.50 ± 0.32 WT vs. 2.94 ± 1.05 FMR-KO) indicating that when distribution of states is taken into account, firing rates are similar in WT and FMR-KO rats. Pair-wise spike rate correlations, however, were different during activation. As expected, restricting pairwise correlation calculations to periods of activation-reduced mean correlations between neurons, and revealed a significant number of anticorrelated neuron pairs (Renart et al. 2010). The proportion of negatively correlated FS × FS pairs (7.4 ± 3.5% WT vs. 16.5 ± 8.7% FMR KO) was not significantly increased. In contrast, RS × RS pairs (6.9 ± 1.6% WT vs. 12.7 ± 1.4 FMR-KO, $P = 0.042$ Bonferroni corrected t-test) and RS × FS pairs (6.2 ± 1.5% WT vs. 32.4 ± 5.4% FMR-KO, $P = 10^{-4}$) showed significant increase in the proportion anticorrelated pairs in FMR-KO rats, suggesting that inhibitory–inhibitory and inhibitory–excitatory connections are specifically affected. The proportion of uncorrelated pairs was similar for RS × RS (46.1 ± 3.2% WT vs. 50.2 ± 1.9 FMR-KO) and RS × FS (39.1 ± 2.8% WT vs. 36.7 ± 3.8% FMR-KO), but increased for FS × FS pairs (23.9 ± 4.2% WT vs. 57.3 ± 8.9% FMR-KO, $P = 0.039$). The proportion of correlated pairs was not significantly reduced for RS × RS (13.0 ± 2.7% WT vs. 4.6 ± 1.7% FMR-KO), but was significantly reduced for RS × FS pairs (23.5 ± 3.8% WT vs. 3.1 ± 3.7% FMR-KO, $P = 0.0012$), and was strongly reduced for FS × FS pairs, which had a large proportion of correlated pairs in wild-type, but few in FMR-KO (46.8 ± 6.2% WT vs. 10.1 ± 3.9% FMR-KO, $P = 10^{-5}$), again suggesting that functional connectivity of interneurons is strongly affected in FMR-KOs.

Together pairwise spike comparisons show that the cortical network in FMR-KO is less synchronized than wild-type, both because they spend more time in the activated, desynchronized state, but also because the network itself has reduced synchronization. Examination of pair-wise comparisons limited to the activate state revealed that functional connections between interneurons are strongly disrupted, likely reducing the effectiveness of the inhibitory drive which can in turn increase time spent in the activated state (Carlen et al. 2012).

Normal Spontaneous Retinal Wave-Driven Activity in FMR-KO Rats before Eye-Opening

Spontaneous, resting cortical activity patterns in P2–11 rats are very different from those observed in the third postnatal week onward. Specifically, there are no active (UP) states, and there is no modulation of visual cortical activity by movement (Colonnese 2014). Instead, spontaneous activity consists of long (10–60 s) silent periods interrupted by clusters of 0.5–2 s bursts of 10–20 Hz oscillation (spindle-bursts) that last a total of 5–10 s. During the first postnatal week, these transients are the result of cholinergic retinal waves reaching cortex (Hanganu et al. 2006), and no other patterns of activity are observed, resulting in a unimodal distribution of event duration with a peak between 1 and 10 s (Colonnese and Khazipov 2010). To determine whether the cortical circuit changes caused by lack of FMRP affect these early patterns, or whether activity changes in FMR-KO rats instead originate with the development of cortical states, we examined event duration as well as the frequency distribution of the superficial layer dEEG in paired littermate controls at P4–5 ($n = 5$ each). Neither the frequency distribution nor event durations were different in FMR-KO rats (Fig. 4A–D), showing that the generation of thalamocortical oscillations in response to retinal waves is normal in FMR-KO, that there is no hyperactivity in visual cortex leading to increased activity between waves, and that there are no novel activity patterns at this age.

During the second postnatal week, spontaneous activity patterns change slightly. Slow activity transients, now driven by glutamatergic retinal waves, continue, but short bursts of activity—likely cortical giant depolarizing potentials (Allene et al. 2008), primitives of the cortical active state (Rochefort et al. 2009)—become common, resulting in a bimodal distribution of event duration (Colonnese and Khazipov 2010). This developmental progression was not altered in FMR-KO. Both the frequency distribution (Fig. 4E) and event duration (Fig. 4F) were similar between wild-type and FMR-KO at P9–11 ($n = 12$ wild-type, 16 FMR-KO), and both groups showed the normal developmental increase in short-duration events as well as a shift to higher frequencies in

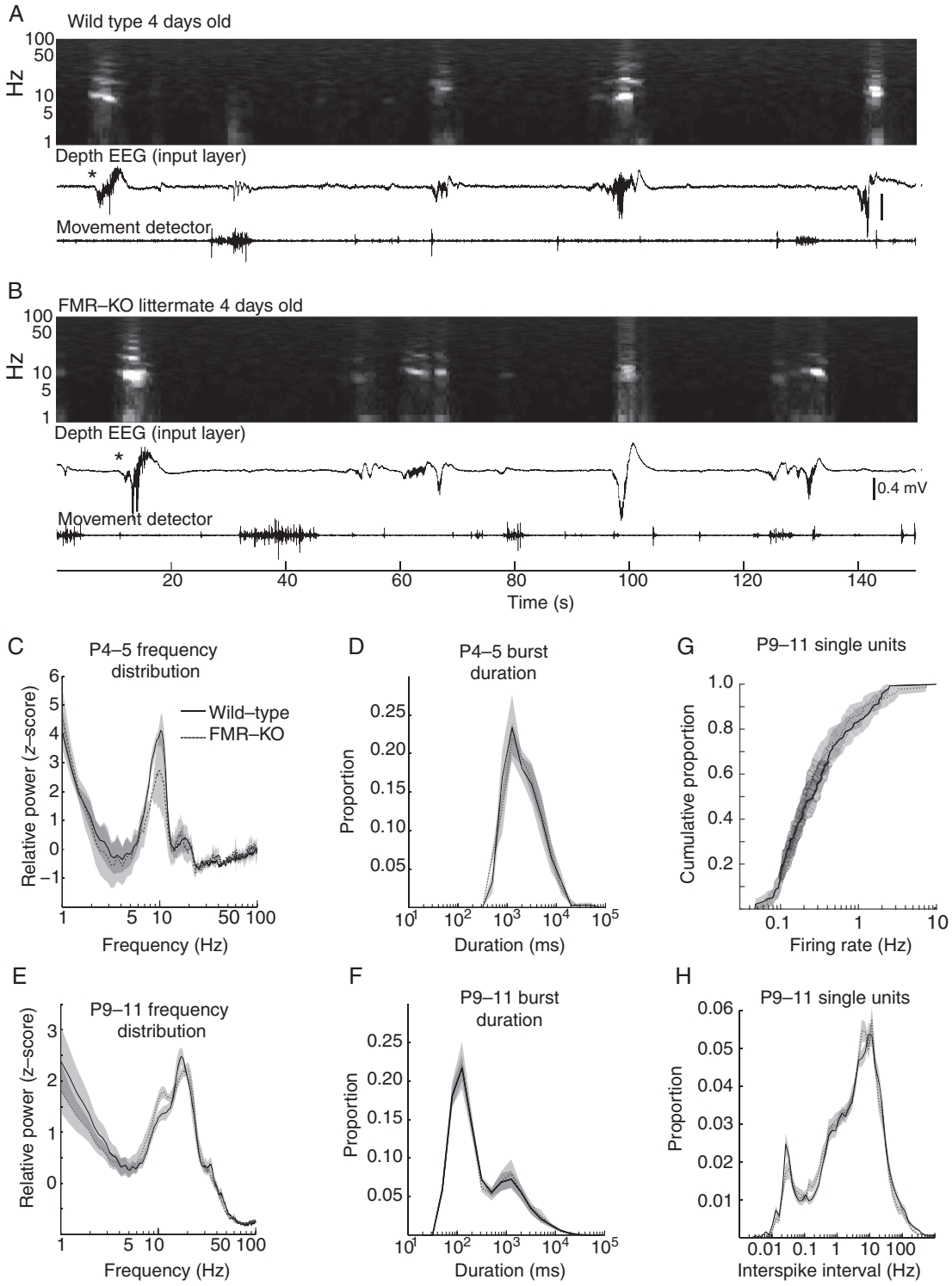

Figure 4. Normal spontaneous activity in infant FMR-KO rats. (*A*,*B*) Example traces and normalized spectrograms of spontaneous activity in 4-day-old littermates (Layer 4). Note the characteristic discontinuous pattern of activity for this age: Silent periods interspersed with "slow activity transients" (bursts of rapid 10–30 Hz oscillations). (*C*) Resting-state spectral analysis for P4–5 wild-type and FMR-KO rats. Plots show population mean frequency distributions. (*D*) Population mean of burst duration for P4–5 animals. (*E*) Mean frequency distribution for P9–11 pups. (*F*) Burst duration for P9–11 animals. (*G*) Cumulative distribution of median single-unit firing rates (P9–11). Shaded area shows 95% confidence intervals. (*H*) Single neuron population mean of the instantaneous firing rate distribution (P9–11). WT = solid black line; FMR-KO dashed line in all panels.

the spectrogram. The absence of major changes in the duration of events and oscillatory behavior of the cortex suggests that the generation of retinal waves and their transmission in the thalamus is largely intact in the FMR-KO.

To examine whether the hyposynchrony and reduced firing observed in juvenile FMR-KO is present in infant animals, we attempted to identify single neurons by spike-sorting during the first 2 postnatal weeks. The proportion of spikes successfully

assigned to good clusters by spike-sorting was insufficient for single-unit analysis at P4–5 (<40%), likely as a result of a smaller signal-to-noise ratio at these ages. By P9–11, spike-sorting assigned a similar proportion of total spikes to well-isolated clusters as in juveniles (>60%, $n = 104$ wild-type, 90 FMR-KO), though they could not be clearly sorted by type. Median firing rates for both groups at this age were approximately 20% of those at P19–24 (0.26 ± 0.04 Hz WT vs. 0.22 ± 0.02 Hz FMR-KO). Neither median firing rates, firing rate distribution (Fig. 4*G*), nor the distribution of interspike intervals (Fig. 4*H*) were different between groups at this age. The proportion of single units with a pair-wise cross-correlation coefficient of zero was similar between groups (data not shown; 51.5 ± 7.8% WT vs. 43.2 ± 6.8% FMR-KO; $P = 0.54$). In total, our data show that immature spontaneous activity patterns are normal in the FMR-KO, and that the alteration in dEEG signal and single-unit spike rate differences are linked to the development of cortical activation states.

Hyposynchrony in the FMR-KO Rat Precedes Deficits in Cortical State Regulation

At what point during development does the reduced synchronization observed in juvenile rats begin? While the single-unit pair-wise cross-correlations at P9–11 show no difference between groups, these correlations are very low relative to juveniles, even for the wild-type animals, suggesting they may not have sufficient resolution to detect subtle differences. Previous reports have observed higher synchronization of cortical activity in wild-type infants than juveniles with both calcium imaging (Golshani et al. 2009; Rochefort et al. 2009) and MUA (Colonnese and Khazipov 2010). We therefore examined the correlations between multiunit spike rate derived from electrodes located in superficial (2–4) and deep (5–6) layers in each of the 3 critical age ranges (P4–5, P9–11, and P19–24) during quiet rest (Fig. 5). As a complement to single-unit pair-wise correlations, multiunit correlation has a number of advantages. It enables measurement of synchronization at P4–5 despite poor clustering of single units at this age. Furthermore, MUA is a more sensitive method for detecting network synchronization when individual units have a low firing probability, or a diverse phase relationship to the oscillation (Fries et al. 2001), and can be applied at all ages.

We observed separate developmental trends in superficial and deep layers. Correlations between electrodes located in superficial layers showed robust synchronization in infant rats, with evidence of an oscillatory component around 10 Hz. The strength of these correlations grew between P4–5 and P9–11. Between the infant and juvenile periods wild-type animals showed slightly reduced zero-phase correlation and elimination of the 10 Hz oscillation, consistent with the loss of spindle-bursts, and the development of the synchronized state. FMR-KO neonates

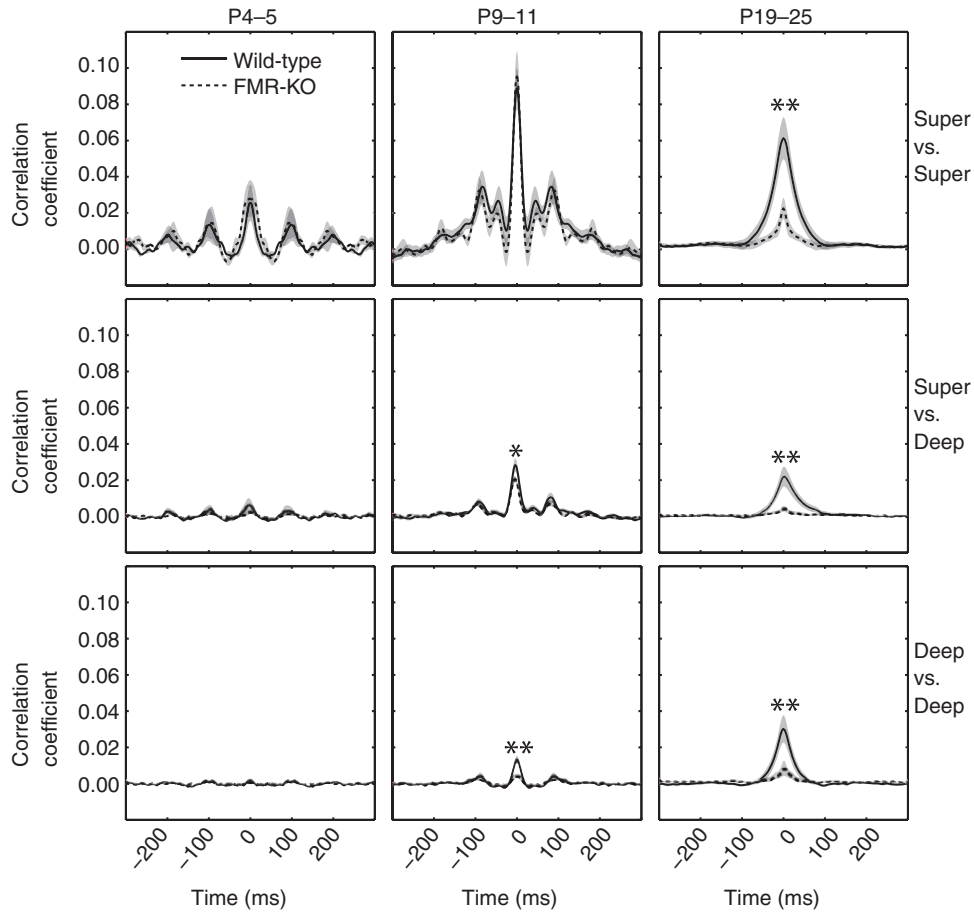

Figure 5. Hyposynchronization in deep layers developmentally precedes cortical state dysregulation in FMR-KO rats. Cross-correlation of multiunit spike rates between electrodes located in super(ficial) (Layers 2–4) and deep (Layers 5–6) cortex for each of the major ages ranges examined. *$P < 0.05$; **$P < 0.01$ measures as the mean correlation coefficients between −10 and +10 ms by *t*-test. Oscillatory cross-correlations in superficial layers at P4–5 and P9–11 result from the retinal wave-driven spindle-bursts present at these ages (Colonnese and Khazipov 2010). Deeper layer correlations develop gradually and are disrupted in FMR-KO rats from the earliest ages they are detectable (P9–11) despite a normal patterning of spontaneous cortical activity (Fig. 4). Wild-type solid black line and FMR-KO dashed line in all panels.

had early (P4–5 and P9–11) oscillatory synchronization similar to wild-type, but FMR-KO juveniles had much weaker zero-phase correlations (mean zero-lag correlation coefficient for wild-type 0.060 ± 0.011, FMR-KO 0.021 ± 0.006 [$P = 0.0017$, t-test]). In contrast to superficial layers, interelectrode correlations in deep layers steadily increased with age in wild-type animals, reflecting the oscillatory engagement of these layers by early network oscillations (Colonnese and Khazipov 2010). FMR-KO rats failed to develop this synchronization in deep layers, resulting in significant differences at both P9–11 (wild-type 0.013 ± 0.002, FMR-KO 0.004 ± 0.001, $P = 0.0024$) and P19–24 (wild-type 0.029 ± 0.007, FMR-KO 0.0080 ± 0.0004, $P = 0.004$).

Together these data show that reduced synchronization caused by lack of FMRP is apparent before the development of prominent changes in cortical dEEG in the third postnatal week, suggesting that hyposynchronization is not caused by the increase in cortical activation; rather, it is a circuit property of FMR-KO rats that contributes to the dEEG changes. Hyposynchronization in infant FMR-KO rats is largely masked by the large oscillatory correlations induced by retinal wave activity during the infant period, which appear unaffected by loss of FMRP.

Discussion

Analysis of the EEG and fMRI signal during rest is a powerful technique to quantify cortical network dynamics and connectivity in human patients (Zhang and Raichle 2010). We have therefore conducted a systematic study of the development of spontaneous "resting state" activity in the visual cortex of the FMR-KO rat. We focused on dEEG because of its sensitivity to detect cortical state modulations in adults (McCormick et al. 2014), early network oscillations in infants (Colonnese and Khazipov 2012), and its potential to be translated into noninvasive diagnostic techniques, such as surface EEG, which could be used for diagnosis or treatment response. We find that cortical activity patterns at developmental ages when spontaneous cortical activity is discontinuous and oscillatory bursts are frequent, which occurs during late gestation in humans (Andre et al. 2010; Colonnese and Khazipov 2012), are largely unaffected by FMRP elimination. Furthermore, the normal transition to mature patterns of continuous activity, including active states, is not delayed. In contrast, we identified the regulation of cortical state by arousal as critically disrupted in FMR-KO rats, an effect that is apparent as soon as cortical activation states arise (P13, just before eye-opening (Colonnese 2014)), and continues through the end of the critical period for ocular dominance plasticity (Fagiolini et al. 1994). The lack of cortical state modulation by movement in FMR-KO rats is a result of a persistent occurrence of the "asynchronous" or "activated" state (Harris and Thiele 2011) during periods of quiet waking, whisking and chewing, when the visual cortex of wild-type rats is dominated by the "synchronized" or "inactivated" state (Hoy and Niell 2015; Vinck et al. 2015). Examination of single and multiunit recordings suggests that changes in local circuitry leading to reduced synchronization between neurons, particularly between inhibitory interneurons, contributes to increased activation in the FMR-KO. Surprisingly, this reduced synchronization develops in deep layers prior to the onset of changes in the cortical dEEG, suggesting that circuit changes in these layers are an important contributor to FMR-KO phenotypes. Together our data provide a novel model to study mechanisms of arousal and attention deficits characteristic of FXS patients, and provide mechanistic insight into reported changes in EEG signals in human patients, as well as suggest an avenue for potential diagnostics at ages before behavioral tests are informative.

Cortical State Regulation, Attention, and Disease

Our findings that cortical activity in FMR-KO rats is disrupted specifically during periods of visual disengagement establish the FMR-KO rat as a potential model of arousal and attention deficits in FXS, as well as for attention deficit disorder and ASD. dEEG modulation in our rats show similar differences from WT as the resting EEG of patients with these disorders. Occipital EEG frequency power in FXS diagnosed children during resting state (eyes closed) is shifted toward frequencies associated with arousal and attention (Van der Molen and Van der Molen 2013). Similar frequency shifts are observed in children with attention deficit disorder. Rather than general arousal increases, these specifically indicate reduced visual attention (Barry et al. 2004). Reports of frequency power shifts in ASD are varied, but many report increased high-frequency and reduced mid-frequency power consistent with a similar increase in cortical activation during rest (Wang et al. 2013). Such direct physiological measurements of cortical arousal and attention may offer an advantage over behavioral measures, which are of necessity confounded by the multiple regions involved in even the simplest behavior, as well as the necessary approximations needed to equate human and animal psychology.

The exact relationship between cortical state modulation in head-fixed rodents and activity modulation by attention in primates remains under investigation. However, the cellular and network similarities between the states engaged by movement and arousal in mice, and the network changes engaged by selective attention in primates (Fries et al. 2001) suggest that many of the same circuits and systems are engaged in both. Thus, cortical activation in rodents is a reasonable model of the cellular and network changes with attention (Harris and Thiele 2011). In mice, activation and the attendant desynchronization of visual cortex is correlated with pupil diameter, believed to reflect systemic arousal (Reimer et al. 2014; Vinck et al. 2015), more so than movement per se. Movement adds increased gamma oscillations and neuronal firing rate to the activation, suggesting the 2 states are dissociable or at least additive. In contrast to previous mouse studies, in our rats, which were head-fixed but not free to run, we observed clear periods of volitional movement and arousal (e.g., whisking, grooming, and chewing) that were not accompanied by activation in wild-type animals, suggesting that activation in visual cortex is driven in part by visual engagement and not simply by systemic arousal.

A number of factors suggest that the failure of FMR-KO rats to modulate dEEG spectra between movement and quiet waking is entirely due to these animals remaining in an activated state (likely similar to the "aroused" state as identified by (Vinck et al. 2015)) during quiet wakefulness. First, low-frequency activity, which is more correlated with pupil dynamics than movement in mice, is primarily affected in FMR-KO rats (e.g., Fig. 1*D*2). Second, spike rates are reduced during "arousal" in mice, and were also reduced in excitatory neurons in FMR-KO rats when measured over all behavioral states. Third, spike rate modulation by movement was intact in FMR-KO rats, suggesting their visual cortex is not simply stuck in the movement-related state. In older mice movement causes increased gamma synchronization, which we did not observe here. This is not surprising, as induced gamma oscillations above 40 Hz develop at ages later than those we examined (Hoy and Niell 2015).

The increased prevalence of cortical activation in the FMR-KO could be due either to increased arousal compared with wild-type in our setup, or to changes in the cortical circuitry of FMR-KO rats, which drive the network toward the asynchronous

state even in the absence of systemic arousal. We favor the latter hypothesis, because we observed differences between genotypes even during an equivalent arousal state—whisking or chewing—when the rats are awake and alert, but not focused on vision. Furthermore, FMR-KO rats did not move or whisk more in our setup, as would be expected if they were more aroused. Finally, two findings have suggested that cortical states in FMR-KO mice are biased toward activation at lower levels of arousal. First, cortical slices and anesthetized mice have longer UP states (Gibson et al. 2008; Hays et al. 2011), which should bias the network toward activation in awake animals. Secondly, reducing arousal with anesthesia has comparatively less effect in FMR-KO mice (Goncalves et al. 2013). Thus, the simplest explanation of these results is that altered network properties of the FMR-KO rat reduce synchronization and make it more difficult to enter into synchronized states for a given level of arousal. This is supported by our data that local networks are hypo-synchronous in FMR-KO even during equivalent states, and that deep layer synchronization is disrupted prior to the development of cortical states (Colonnese 2014).

A reduced ability to deactivate cortex is likely to have profound consequences for the attentional regulation of visual processing. In monkeys, directing attention outside of a region's receptive field results in increased low-frequency and reduced high-frequency synchronization (Fries et al. 2001), similar to the deactivation described here. Increased thresholds to deactivate would be expected to contribute to the attentional deficits observed in FXS infants (Scerif et al. 2004; Cornish et al. 2007) as well as in ASD (Marco et al. 2011), as they would be unable to reduce focus on stimuli to which a control infant would not attend, leading to perseveration, reduced top-down control, and sensory over excitation. In addition to visual deficits, failure to properly minimize sensory input when appropriate, for example when concentrating or resting, is a potential mechanism for the sensory hypersensitivity and hyperarousal common in these patients.

Synaptic and Circuit Mechanisms of State Dysfunction

Understanding how dysregulated gene expression following loss of FMRP causes the individual phenotypes of the disorder is a key step in designing novel treatments (Krueger and Bear 2011). Determining how network properties are altered in syndromic causes of neural disorders is important, because these properties may form "nodes" by which diverse gene disruptions cause similar symptoms in nonsyndromic forms. FMRP deletion induces a complex series of synaptic and cellular changes that increase excitability of excitatory neurons and reduce the effectiveness of inhibition, suggesting that a net increase of cortical excitability is a node for both FXS (Contractor et al. 2015) as well as ASD (Rubenstein and Merzenich 2003; Markram et al. 2007). At the network level, hyperexcitable phenotypes are common, including exaggerated sensory responses (Rotschafer and Razak 2013; Arnett et al. 2014; Zhang et al. 2014) and seizure susceptibility (Yan et al. 2004; Michalon et al. 2012), which likely contribute to sensory hypersensitivity and increased seizure incidence in FXS (Hagerman and Hagerman 2002).

The increased prevalence of activation we observed is an expected outcome of reduced drive to inhibitory neurons (Carlen et al. 2012); however, experiments and modeling also suggest that reduced inhibition could yield a similar effect (Sanchez-Vives et al. 2010; Renart et al. 2010). The former is the likely contributor here, as excitatory drive to FS neurons (Patel et al. 2013), their inhibitory driving force (He et al. 2014; Tyzio et al. 2014) and their density (Selby et al. 2007) is reduced in FMR-KO mice. In addition, the synchronization of inhibitory interneurons that act to suppress the activated state (which have spike durations of intermediate duration and are likely included in our FS group) is also disturbed in FMR-KO mice (Paluszkiewicz et al. 2011). Our single-unit correlations suggest that correlations between FS neurons are particularly affected, supporting inhibitory dysfunction as contributing to the phenotype. Along with reduced drive to inhibitory neurons, layer 5 neurons with FMR-KO are hyperconnected to each other, and this connectivity also contributes to elongated active states in vitro (Gibson et al. 2008; Hays et al. 2011; Patel et al. 2014).

Goncalves et al. (2013), examining superficial layers of somatosensory cortex at similar ages did not observe changes in the distribution of cortical states, but instead found increased firing and hyper-synchrony during synchronized states, network effects seemingly opposite from ours. However, synchronization was measured horizontally by calcium imaging, which reflects primarily bursts of action potentials on a slow (100 ms plus) time scale. We measured vertical synchronization based on single spikes on a fast (20 ms) time scale, with the effect of shared slow correlations removed. Developmental reductions of slow horizontal correlation and increased fast vertical correlation actually occur at the same age in visual cortex (Rochefort et al. 2009); Fig. 5). The absence of a disruption in cortical state regulation in somatosensory cortex may be a result of differences in the regulation of active state between regions. In mouse barrel cortex, activated states are strongly associated with whisking (Poulet and Petersen 2008), and it is unclear if there exists a "covert" arousal state present in the absence of whisking, similar to the aroused state seen in the absence of movement in V1 (Reimer et al. 2014; Vinck et al. 2015). Interestingly, neither study showed increased FMR-KO firing during the activated state, suggesting that hyperexcitability of cortical circuits may contribute to the prevalence of activation, but is not a core feature of activity during aroused states.

Together the present study extends this prior work on the cellular and network effects of FMR-KO by demonstrating that the regulation of cortical active states is a common (if varied in expression (Motanis and Buonomano 2015)) feature of FMRP deletion in mice and rats. Previously, it was unclear whether changes in excitability limited to quiescent states contribute to waking phenotypes. Our results suggest a mechanism for this, namely that an increased propensity of local circuits to enter or maintain active states results in a failure to appropriately deactivate cortex in the absence of attention and arousal.

Early Developmental Activity and FXS

Disruption of cortical activity in the FMR-KO began around eye-opening, the age at which cortical active states develop (Colonnese 2014). Prior to this, during the first 2 postnatal weeks, the cortex does not generate active states and is largely silent (Hanganu et al. 2006; Colonnese and Khazipov 2010). Activity comes as bursts of spindle shaped oscillations called "spindle-bursts," the rodent homolog of "delta-brushes" observed spontaneously in the EEGs of preterm infants (Colonnese and Khazipov 2012). In visual cortex, spindle-bursts are largely patterned by feed-forward thalamic oscillations driven by spontaneous retinal waves (Colonnese and Khazipov 2010; Minlebaev et al. 2011; Ackman et al. 2012). We could detect no difference in the spindle oscillations of FMR-KOs, their duration nor their occurrence, nor changes in the single-unit firing patterns of neurons during this time. This strongly suggests that retinal wave generation and transmission in the thalamus is normal in FMR-KO rats. It is

perhaps surprising to find minimal disruption of activity at this time, as multiple circuit and synaptic disruptions are more severe during development (Contractor et al. 2015), particularly depolarizing GABA (He et al. 2014) which should increase excitability at these ages. However, cortical GABAergic inhibition plays little role in patterning spindle-bursts (Minlebaev et al. 2007; Colonnese et al. 2010).

What changes around eye-opening allows low FMRP levels to begin affecting cortical activity? First, there is the development of rapid inhibition (Colonnese 2014)—which is critical to maintenance of UP states (Haider et al. 2006)—likely through potentiation of thalamic synapses on FS interneurons (Chittajallu and Isaac 2010), the drive to which is disrupted in FMR-KO rats (Patel et al. 2013). Second, there is an increase in spontaneous firing, UP states appear, and cortical activation begins to occur during movement (Colonnese 2014). Thus, emergence of cortical activity disruption in FMR-KO is linked to the generation and regulation of activity states dependent on recurrent activity, particularly in deep layers (Sanchez-Vives and McCormick 2000). Some of the circuit defects that cause changes in UP states appear to predate their appearance. Neurons in deep layers were significantly less synchronized by the second postnatal week, possibly as a result of layer 5 hypoconnectivity (Patel et al. 2014). However, because synchronization in superficial layers is driven by thalamic input, not intracortical connections (Colonnese and Khazipov 2010), FMR-KO-induced desynchronization of superficial layers does not become apparent until intracortical connections dominate spontaneous activity around eye-opening.

Together, our recordings from neonatal rats revealed 3 key findings. First, development of cortical activity in Fragile X rats is not delayed, and there are no early activity defects that are later reversed, despite a normally high expression of FMRP and synaptic and cellular defects in FMR-KO rats at these ages (Till et al. 2012; Contractor et al. 2015). Rather, cortical activity during a time period (P5–11) when visual cortical activity is similar to that observed during human late gestation (Colonnese and Khazipov 2012) appears normal, and hyposynchrony we observed at these ages is progressive. This offers hope neural deficits could be prevented in patients if treated early.

Second, effects of FMR-KO on spontaneous activity are correlated with the onset of activity patterns dependent on intracortical recurrent circuitry, which are minimal or absent in visual cortex at early ages (Rochefort et al. 2009; Colonnese 2014). Disruption of activity in the somatosensory cortex of FMR-KO mice develops along a similar time course (Golshani et al. 2009; Goncalves et al. 2013). Interestingly, these processes are not delayed by FMR-KO in vivo as they are in vitro (Motanis and Buonomano 2015), suggesting circuit mechanisms of compensation are important factors in the expression of the disease in vivo (Ben-Ari 2008).

Finally, in addition to identifying cortical circuit defects in FXS, our results provide inspiration for assays that could be used to predict responses to treatment in human infants. Changes in evoked and spontaneous activity suggest that birth in humans and eye-opening in rats are homologous developmental points in visual cortex (Colonnese et al. 2010; Andre et al. 2010). Thus, if human infants with FXS express similar changes in neural activity our results predict they should be detectable at birth or soon after, before FXS is typically diagnosed between 9 and 35 months (Mirrett et al. 2004; Bailey et al. 2009).

Funding

This work was supported by grants from the National Eye Institute at the National Institutes of Health (EY022730) and National Center for Advancing Translational Sciences to MTC, and a gift from Dr Jack and Shirley Kaplan to G.W.U. Its contents are solely the responsibility of the authors and do not necessarily represent the official views of the Sponsors.

Notes

Conflict of Interest: None declared.

References

Ackman JB, Burbridge TJ, Crair MC. 2012. Retinal waves coordinate patterned activity throughout the developing visual system. Nature. 490(7419):219–225.

Allene C, Cattani A, Ackman JB, Bonifazi P, Aniksztejn L, Ben-Ari Y, Cossart R. 2008. Sequential generation of two distinct synapse-driven network patterns in developing neocortex. J Neurosci. 28(48):12851–12863.

Andre M, Lamblin MD, d'Allest AM, Curzi-Dascalova L, Moussalli-Salefranque F, S Nguyen The T, Vecchierini-Blineau MF, Wallois F, Walls-Esquivel E, Plouin P. 2010. Electroencephalography in premature and full-term infants. Developmental features and glossary. Neurophysiol Clin. 40(2):59–124.

Arnett MT, Herman DH, McGee AW. 2014. Deficits in tactile learning in a mouse model of fragile X syndrome. PLoS One. 9(10): e109116.

Bailey DB Jr, Raspa M, Bishop E, Holiday D. 2009. No change in the age of diagnosis for fragile x syndrome: findings from a national parent survey. Pediatrics. 124(2):527–533.

Barry RJ, Clarke AR, McCarthy R, Selikowitz M, Rushby JA, Ploskova E. 2004. EEG differences in children as a function of resting-state arousal level. Clin Neurophysiol. 115(2):402–408.

Ben-Ari Y. 2008. Neuro-archaeology: pre-symptomatic architecture and signature of neurological disorders. Trends Neurosci. 31(12):626–636.

Carlen M, Meletis K, Siegle JH, Cardin JA, Futai K, Vierling-Claassen D, Ruhlmann C, Jones SR, Deisseroth K, Sheng M, et al. 2012. A critical role for NMDA receptors in parvalbumin interneurons for gamma rhythm induction and behavior. Mol Psychiatry. 17(5):537–548.

Chittajallu R, Isaac JT. 2010. Emergence of cortical inhibition by coordinated sensory-driven plasticity at distinct synaptic loci. Nat Neurosci. 13(10):1240–1248.

Cohen MX. 2014. Analyzing neural time series data: theory and practice. Cambridge (MA): MIT Press.

Colonnese M, Khazipov R. 2012. Spontaneous activity in developing sensory circuits: implications for resting state fMRI. Neuroimage. 62(4):2212–2221.

Colonnese MT. 2014. Rapid developmental emergence of stable depolarization during wakefulness by inhibitory balancing of cortical network excitability. J Neurosci. 34(16):5477–5485.

Colonnese MT, Kaminska A, Minlebaev M, Milh M, Bloem B, Lescure S, Moriette G, Chiron C, Ben-Ari Y, Khazipov R. 2010. A conserved switch in sensory processing prepares developing neocortex for vision. Neuron. 67(3):480–498.

Colonnese MT, Khazipov R. 2010. "Slow activity transients" in infant rat visual cortex: a spreading synchronous oscillation patterned by retinal waves. J Neurosci. 30(12):4325–4337.

Contractor A, Klyachko VA, Portera-Cailliau C. 2015. Altered neuronal and circuit excitability in fragile X syndrome. Neuron. 87 (4):699–715.

Cornish K, Scerif G, Karmiloff-Smith A. 2007. Tracing syndrome-specific trajectories of attention across the lifespan. Cortex. 43 (6):672–685.

Cornish K, Sudhalter V, Turk J. 2004. Attention and language in fragile X. Ment Retard Dev Disabil Res Rev. 10(1):11–16.
Darnell JC, Klann E. 2013. The translation of translational control by FMRP: therapeutic targets for FXS. Nat Neurosci. 16 (11):1530–1536.
Fagiolini M, Pizzorusso T, Berardi N, Domenici L, Maffei L. 1994. Functional postnatal development of the rat primary visual cortex and the role of visual experience: dark rearing and monocular deprivation. Vision Res. 34(6):709–720.
Fries P, Reynolds JH, Rorie AE, Desimone R. 2001. Modulation of oscillatory neuronal synchronization by selective visual attention. Science. 291(5508):1560–1563.
Gibson JR, Bartley AF, Hays SA, Huber KM. 2008. Imbalance of neocortical excitation and inhibition and altered UP states reflect network hyperexcitability in the mouse model of fragile X syndrome. J Neurophysiol. 100(5):2615–2626.
Golshani P, Gonsalves JT, Khoshkhoo S, Mostany R, Smirnakis S, Portera-Cailliau C. 2009. Internally mediated developmental desynchronization of neocortical network activity. J Neurophysiol. 29(35):10890–9.
Goncalves JT, Anstey JE, Golshani P, Portera-Cailliau C. 2013. Circuit level defects in the developing neocortex of fragile X mice. Nat Neurosci. 16(7):903–909.
Hagerman RJ, Hagerman PJ. 2002. Fragile x syndrome: diagnosis, treatment, and research. 3rd ed. Baltimore: Johns Hopkins University Press.
Haider B, Duque A, Hasenstaub AR, McCormick DA. 2006. Neocortical network activity in vivo is generated through a dynamic balance of excitation and inhibition. J Neurosci. 26(17):4535–4545.
Haider B, McCormick DA. 2009. Rapid neocortical dynamics: cellular and network mechanisms. Neuron. 62(2):171–189.
Hamilton SM, Green JR, Veeraragavan S, Yuva L, McCoy A, Wu Y, Warren J, Little L, Ji D, Cui X, et al. 2014. Fmr1 and Nlgn3 knockout rats: novel tools for investigating autism spectrum disorders. Behav Neurosci. 128(2):103–109.
Hanganu IL, Ben-Ari Y, Khazipov R. 2006. Retinal waves trigger spindle bursts in the neonatal rat visual cortex. J Neurosci. 26(25):6728–6736.
Harris KD, Thiele A. 2011. Cortical state and attention. Nat Rev Neurosci. 12(9):509–523.
Hays SA, Huber KM, Gibson JR. 2011. Altered neocortical rhythmic activity states in Fmr1 KO mice are due to enhanced mGluR5 signaling and involve changes in excitatory circuitry. J Neurosci. 31(40):14223–14234.
He Q, Nomura T, Xu J, Contractor A. 2014. The developmental switch in GABA polarity is delayed in fragile X mice. J Neurosci. 34(2):446–450.
Herculano-Houzel S, Munk MH, Neuenschwander S, Singer W. 1999. Precisely synchronized oscillatory firing patterns require electroencephalographic activation. J Neurosci. 19 (10):3992–4010.
Hoy JL, Niell CM. 2015. Layer-specific refinement of visual cortex function after eye opening in the awake mouse. J Neurosci. 35 (8):3370–3383.
Jacquemont S, Hagerman RJ, Hagerman PJ, Leehey MA. 2007. Fragile-X syndrome and fragile X-associated tremor/ataxia syndrome: two faces of FMR1. Lancet Neurol. 6:45–55.
Kadir SN, Goodman DF, Harris KD. 2014. High-dimensional cluster analysis with the masked EM algorithm. Neural Comput. 26(11):2379–2394.
Kramvis I, Mansvelder HD, Loos M, Meredith R. 2013. Hyperactivity, perseveration and increased responding during attentional rule acquisition in the fragile X mouse model. Front Behav Neurosci. 7:172.
Krueger DD, Bear MF. 2011. Toward fulfilling the promise of molecular medicine in fragile X syndrome. Annu Rev Med. 62:411–429.
Krueger DD, Osterweil EK, Chen SP, Tye LD, Bear MF. 2011. Cognitive dysfunction and prefrontal synaptic abnormalities in a mouse model of fragile X syndrome. Proc Natl Acad Sci USA. 108(6):2587–2592.
Marco EJ, Hinkley LB, Hill SS, Nagarajan SS. 2011. Sensory processing in autism: a review of neurophysiologic findings. Pediatr Res. 69(5 Pt 2):48R–54R.
Markram H, Rinaldi T, Markram K. 2007. The intense world syndrome–an alternative hypothesis for autism. Front Neurosci. 1(1):77–96.
McCormick DA, McGinley MJ, Salkoff DB. 2014. Brain state dependent activity in the cortex and thalamus. Curr Opin Neurobiol. 31C:133–140.
Meredith RM, Dawitz J, Kramvis I. 2012. Sensitive time-windows for susceptibility in neurodevelopmental disorders. Trends Neurosci. 35(6):335–344.
Michalon A, Sidorov M, Ballard TM, Ozmen L, Spooren W, Wettstein JG, Jaeschke G, Bear MF, Lindemann L. 2012. Chronic pharmacological mGlu5 inhibition corrects fragile X in adult mice. Neuron. 74(1):49–56.
Minlebaev M, Ben-Ari Y, Khazipov R. 2007. Network mechanisms of spindle-burst oscillations in the neonatal rat barrel cortex in vivo. J Neurophysiol. 97(1):692–700.
Minlebaev M, Colonnese M, Tsintsadze T, Sirota A, Khazipov R. 2011. Early gamma oscillations synchronize developing thalamus and cortex. Science. 334(6053):226–229.
Mirrett PL, Bailey DB Jr, Roberts JE, Hatton DD. 2004. Developmental screening and detection of developmental delays in infants and toddlers with fragile X syndrome. J Dev Behav Pediatr. 25(1):21–27.
Mitra P, Bokil H. 2007. Observed brain dynamics. New York: Oxford University Press, USA.
Moon J, Beaudin AE, Verosky S, Driscoll LL, Weiskopf M, Levitsky DA, Crnic LS, Strupp BJ. 2006. Attentional dysfunction, impulsivity, and resistance to change in a mouse model of fragile X syndrome. Behav Neurosci. 120(6):1367–1379.
Moon J, Ota KT, Driscoll LL, Levitsky DA, Strupp BJ. 2008. A mouse model of fragile X syndrome exhibits heightened arousal and/or emotion following errors or reversal of contingencies. Dev Psychobiol. 50(5):473–485.
Motanis H, Buonomano D. 2015. Delayed in vitro development of up states but normal network plasticity in fragile X circuits. Eur J Neurosci. 42(6):2312–2321.
Niell CM, Stryker MP. 2010. Modulation of visual responses by behavioral state in mouse visual cortex. Neuron. 65(4):472–479.
Paluszkiewicz SM, Olmos-Serrano JL, Corbin JG, Huntsman MM. 2011. Impaired inhibitory control of cortical synchronization in fragile X syndrome. J Neurophysiol. 106(5):2264–2272.
Patel AB, Hays SA, Bureau I, Huber KM, Gibson JR. 2013. A target cell-specific role for presynaptic Fmr1 in regulating glutamate release onto neocortical fast-spiking inhibitory neurons. J Neurosci. 33(6):2593–2604.
Patel AB, Loerwald KW, Huber KM, Gibson JR. 2014. Postsynaptic FMRP promotes the pruning of cell-to-cell connections among pyramidal neurons in the L5A neocortical network. J Neurosci. 34(9):3413–3418.
Pearce PS, Friedman D, Lafrancois JJ, Iyengar SS, Fenton AA, Maclusky NJ, Scharfman HE. 2014. Spike-wave discharges in adult sprague-dawley rats and their implications for animal models of temporal lobe epilepsy. Epilepsy Behav. 32:121–131.
Polack PO, Friedman J, Golshani P. 2013. Cellular mechanisms of brain state-dependent gain modulation in visual cortex. Nat Neurosci. 16(9):1331–1339.

Poulet JF, Petersen CC. 2008. Internal brain state regulates membrane potential synchrony in barrel cortex of behaving mice. Nature. 454(7206):881–885.

Reimer J, Froudarakis E, Cadwell CR, Yatsenko D, Denfield GH, Tolias AS. 2014. Pupil fluctuations track fast switching of cortical states during quiet wakefulness. Neuron. 84(2): 355–362.

Renart A, de la Rocha J, Bartho P, Hollender L, Parga N, Reyes A, Harris KD. 2010. The asynchronous state in cortical circuits. Science. 327(5965):587–590.

Roberts JE, Hatton DD, Long AC, Anello V, Colombo J. 2012. Visual attention and autistic behavior in infants with fragile X syndrome. J Autism Dev Disord. 42(6):937–946.

Rochefort NL, Garaschuk O, Milos R, Narushima M, Marandi N, Pichler B, Kovalchuk Y, Konnerth A. 2009. Sparsification of neuronal activity in the visual cortex at eye-opening. Proc Natl Acad Sci USA. 106(35):15049–15054.

Rotschafer S, Razak K. 2013. Altered auditory processing in a mouse model of fragile X syndrome. Brain Res. 1506:12–24.

Rubenstein JL, Merzenich MM. 2003. Model of autism: increased ratio of excitation/inhibition in key neural systems. Genes Brain Behav. 2(5):255–267.

Sanchez-Vives MV, Mattia M, Compte A, Perez-Zabalza M, Winograd M, Descalzo VF, Reig R. 2010. Inhibitory modulation of cortical up states. J Neurophysiol. 104(3):1314–1324.

Sanchez-Vives MV, McCormick DA. 2000. Cellular and network mechanisms of rhythmic recurrent activity in neocortex. Nat Neurosci. 3(10):1027–1034.

Scerif G, Cornish K, Wilding J, Driver J, Karmiloff-Smith A. 2004. Visual search in typically developing toddlers and toddlers with Fragile X or Williams syndrome. Dev Sci. 7(1):116–130.

Schmitzer-Torbert N, Jackson J, Henze D, Harris K, Redish AD. 2005. Quantitative measures of cluster quality for use in extracellular recordings. Neuroscience. 131(1):1–11.

Selby L, Zhang C, Sun QQ. 2007. Major defects in neocortical GABAergic inhibitory circuits in mice lacking the fragile X mental retardation protein. Neurosci Lett. 412(3):227–232.

Solnik S, Rider P, Steinweg K, DeVita P, Hortobagyi T. 2010. Teager-Kaiser energy operator signal conditioning improves EMG onset detection. Eur J Appl Physiol. 110(3):489–498.

Steriade M, Contreras D, Amzica F. 1994. Synchronized sleep oscillations and their paroxysmal developments. Trends Neurosci. 17(5):199–208.

Till SM, Asiminas A, Jackson AD, Katsanevaki D, Barnes SA, Osterweil EK, Bear MF, Chattarji S, Wood ER, Wyllie DJ, et al. 2015. Conserved hippocampal cellular pathophysiology but distinct behavioural deficits in a new rat model of FXS. Hum Mol Genet. 24(21):5977–5984.

Till SM, Wijetunge LS, Seidel VG, Harlow E, Wright AK, Bagni C, Contractor A, Gillingwater TH, Kind PC. 2012. Altered maturation of the primary somatosensory cortex in a mouse model of fragile X syndrome. Hum Mol Genet. 21(10):2143–2156.

Tyzio R, Nardou R, Ferrari DC, Tsintsadze T, Shahrokhi A, Eftekhari S, Khalilov I, Tsintsadze V, Brouchoud C, Chazal G, et al. 2014. Oxytocin-mediated GABA inhibition during delivery attenuates autism pathogenesis in rodent offspring. Science. 343(6171):675–679.

Van der Molen MJ, Van der Molen MW. 2013. Reduced alpha and exaggerated theta power during the resting-state EEG in fragile X syndrome. Biol Psychol. 92(2):216–219.

Vinck M, Batista-Brito R, Knoblich U, Cardin JA. 2015. Arousal and locomotion make distinct contributions to cortical activity patterns and visual encoding. Neuron. 86(3):740–754.

Wang J, Barstein J, Ethridge LE, Mosconi MW, Takarae Y, Sweeney JA. 2013. Resting state EEG abnormalities in autism spectrum disorders. J Neurodev Disord. 5(1):24:1955-5-24.

Wijetunge LS, Chattarji S, Wyllie DJ, Kind PC. 2013. Fragile X syndrome: from targets to treatments. Neuropharmacology. 68:83–96.

Yan QJ, Asafo-Adjei PK, Arnold HM, Brown RE, Bauchwitz RP. 2004. A phenotypic and molecular characterization of the Fmr1-tm1Cgr fragile X mouse. Genes Brain Behav. 3(6):337–359.

Zhang Y, Bonnan A, Bony G, Ferezou I, Pietropaolo S, Ginger M, Sans N, Rossier J, Oostra B, LeMasson G, et al. 2014. Dendritic channelopathies contribute to neocortical and sensory hyperexcitability in Fmr1(-/y) mice. Nat Neurosci. 17(12):1701–1709.

Zhang D, Raichle ME. 2010. Disease and the brain's dark energy. Nat Rev Neurol. 6(1):15–28.

Zwaigenbaum L, Bryson S, Rogers T, Roberts W, Brian J, Szatmari P. 2005. Behavioral manifestations of autism in the first year of life. Int J Dev Neurosci. 23(2–3):143–152.